Energy Flow Optimization of Integrated Gas and Power Systems in Continuous Time and Space

Zheng, Chao; Fang, Jiakun; Wang, Shaorong; Ai, Xiaomeng; Liu, Zhou; Chen, Zhe

Published in:
IEEE Transactions on Smart Grid

DOI (link to publication from Publisher):
10.1109/TSG.2020.3044609

Publication date:
2021

Document Version
Accepted author manuscript, peer reviewed version

Energy Flow Optimization of Integrated Gas and Power Systems in Continuous Time and Space

Chao Zheng, Jiakun Fang, *Senior Member, IEEE*, Shaorong Wang, Xiaomeng Ai, *Member, IEEE*, Zhou Liu, *Senior Member, IEEE*, Zhe Chen, *Fellow, IEEE*

***Abstract*—Due to the increasing penetration of gas-fired units and power to gas facilities, the electrical power system and natural gas system are more and more bi-directionally coupled. To tackle the challenges on the optimal scheduling operation of an integrated gas and power systems (IGPS), this paper focuses on developing a novel approach to build a continuous spatial-temporal optimal operation schedule model. In the light of different time constants of the electrical power and natural gas systems, the continuous spatial-temporal optimal operation schedule model of IGPS is formulated in function space. Additionally, Bernstein polynomials are used to reformulate the continuous spatial-temporal optimization problem of IGPS to mixed-integer linear programming. In the study cases, the simulation results of a simple integrated system and a combined IEEE 39-bus power system and Belgian natural gas network demonstrate the accuracy and effectiveness of the proposed model.**

***Index Terms*—Integrated gas and power systems, dynamic gas flow, optimal scheduling operation, wind power, function space.**

NOMENCLATURE

Abbreviations

GFU	Gas-fired unit.
CFU	Coal-fired unit.
IGPS	Integrated gas and power system.
EPS	Electrical power system.
NGS	Natural gas system.
P2G	Power to gas.
MFR	Mass flow rate.
AE	Algebraic equation.
PDE	Partial differential equation.

Electrical Power System

$\mathbf{G}_{k,\tau}$	The coeff. of real power of the kth unit on the interval $[t,t+1]$, $\mathbf{G}_{k,\tau}=[G^1_{k,\tau}\ G^2_{k,\tau}\ G^3_{k,\tau}\ G^4_{k,\tau}]^{\mathrm{T}}\in\mathbb{R}^{4\times1}$.
$\boldsymbol{\theta}_{i,\tau}$	The coeff. of voltage phase angle at the bus i on the interval $[t,t+1]$, $\boldsymbol{\theta}_{k,\tau}\in\mathbb{R}^{4\times1}$.
X_{ij}	Line impedance from bus i to j.
$\underline{G}_k$, $\overline{G}_k$	The min. and max. output of the kth unit.
$\mathbf{P}_{ij,\tau}$	The coeff. of the real power flow through line ij on the interval $[t,t+1]$, $\mathbf{P}_{ij,\tau}\in\mathbb{R}^{4\times1}$.
$\overline{P}_{ij}$	The thermal limit of line ij.
R^U_k	The ramp up limit of the kth unit.
R^D_k	The ramp down limit of the kth unit.
R^{SU}_k	The startup ramp limit of the kth unit.
R^{SD}_k	The shutdown ramp limit of the kth unit.
$\mathbf{L}_{i,\tau}$	The coeff. of load profile at bus ith on the interval $[t,t+1]$, $\mathbf{L}_{i,\tau}\in\mathbb{R}^{4\times1}$.
$\mathbf{I}_{k,\tau}$	Commitment variable of the kth unit on the interval $[t,t+1]$, $\mathbf{I}_{k,\tau}=[1_{k,\tau}\ 1_{k,\tau}\ 1_{k,\tau}\ 1_{k,\tau+1}]^{\mathrm{T}}\in\mathbb{R}^{4\times1}$.
$c_{k,\tau}$	The min. cost of kth unit on the interval $[t,t+1]$.
$\alpha_{k,m}$	The cost coeff. of mth section output of the kth unit.
$\overline{C_{k,\tau}}$	The startup cost of the kth unit at the tine t.
$\underline{C_{k,\tau}}$	The shutdwon cost of the kth unit at the tine t.
Ω_{ps}	The set of generations in power systems.
$C_{ps}(\cdot)$	The cost function of the generation units.

Natural Gas System

$\boldsymbol{M}_{n,\tau}$	The coeff. of mass flow rate of nth pipeline on the interval $[t,t+1]$ in Bernstein space, $\boldsymbol{M}_{n,\tau}\in\mathbb{R}^{4\times4}$.
$\boldsymbol{\rho}_{n,\tau}$	The coeff. of gas density of nth pipeline on the interval $[t,t+1]$ in Bernstein space, $\boldsymbol{\rho}_{n,\tau}\in\mathbb{R}^{4\times4}$.
λ	The friction factor.
ω	The gas flow velocity in pipeline (m/s).
d, l, A	The diameter (m), length (m), and cross-sectional area (m^3) of pipeline.
M,ρ	The mass flow rate and density.
$\overline{M}_n$,$\overline{\rho}_n$	The mass flow rate and density limit of nth pipeline.
$\beta_{s,\tau}$	The gas price of sth source on the interval $[t,t+1]$.
Ω_{gs}	The set of source node in gas systems.
$C_{gs}(\cdot)$	The cost function of the natural gas.

Subscripts & Indices

$\mathbb{R}$	Real number.
τ	Index of the τ-th period, *i.e.*,$[t,t+1]$.
x,t	Distance and time, respectively.
T_N	Total time horizon.

This work is supported by the National Key Research and Development Program of China under Grant 2017YFB0902800, and the the Science & Technology Project of State Grid Corporation of China under Grant 52094017003D. (*Corresponding author: Jiakun Fang*, email:jfa@hust.edu.cn)

C. Zheng is with the School of Electrical and Electronic Engineering, Huazhong University of Science and Technology, Wuhan 430074, China, and the Electric Power Dispatch and Control Center, Yunnan Power Grid Co Ltd, Kunming 650011, China. (email:kmzc1991@gmail.com).

J. Fang, S. Wang and X. Ai are with the State Key Laboratory of Advanced Electromagnetic Engineering and Technology, and School of Electrical and Electronic Engineering, Huazhong University of Science and Technology, Wuhan 430074, China. (emails:jfa@hust.edu.cn;wsrwy96@vip.sina.com;xiaomengai@hust.edu.cn).

Z. Chen and Z. Liu are with the Department of Energy Techonology, Aalborg University, Aalborg East 9220, Denmark. (emails:zch@et.aau.dk;zli@et.aau.dk)

N_b, i, j Index of bus in power grid.
m Index of load in power grid.
k Index of generator in power gird.
n Index of pipeline in natural gas system.
N_g Total number of generation.
N_s Total number of source node in gas systems.

I. Introduction

INTEGRATING multi-energy systems, *e.g.*, electricity, natural gas, heat, cooling, and electrified transport, is a strategically crucial technical routine for the emission targets of greenhouse gas and the evolution of energy mix [1]–[5]. In multi-energy systems, the advantages of various energy systems could be fully exploited, such as the efficiency of energy utilization could be improved by jointly operating the multi-energy systems [6], the reliability and flexibility of different energy networks could be coordinated by utilizing the synergies in production, transmission, storage, and consumption [7].

Among different energy sectors, electrical power systems (EPS) and natural gas systems (NGS) are the most common options for bulk energy delivery over a long distance. To construct low-carbon power systems, a number of retired coal-fired units (CFUs) have been replaced with renewable turbines and gas-fired units (GFUs) *in situ* over the past few years [8]–[10]. Meanwhile, with the technological improvement and development, the power to gas (P2G) facilities are a potential choice to reduce the renewable energy sources (RES) curtailment by storing the productions of surplus RES in natural gas pipelines [11], [12]. By means of both the GFUs and P2G facilities, EPS and NGS are tightly and bi-directionally linked, then an integrated gas and power system (IGPS) is formed.

Due to the growing interdependence of IGPS [13]–[15], the topic about optimal planning and scheduling operation of IGPS with considering their interdependence has attracted wide attention from both academia and industry. For the coordinated planning goals, the planning models of IGPS are presented in [16]–[18]. To take into account the generation constraints influenced by the natural gas networks, the security constraints imposed by the natural gas networks are developed and embedded in the unit commitment models [19]–[21]. The physical characteristics of natural gas networks, *e.g.*, linepack, are formulated for the day-ahead operation strategies of IGPS in [22]. Due to the emerging of P2G facilities, the operation strategies of bi-directional energy flow in IGPS are studied in [23], [24]. Under the marketing environment, [25] demonstrates that energy cost distortion was caused by ignoring the natural gas network limitations. In [26], the day-ahead optimal scheduling operation of IGPS is modeled with considering demand response. In most of the reported works, researchers have employed a steady-state gas flow model based on Weymouth equations to formulate the optimal planning and scheduling operation models of IGPS, but the different time scales of EPS and NGS have been neglected in such models. Due to the comparable time scales between NGS and scheduling operations [27], but the distinguishing time constants between EPS and NGS [28], the reported state-of-the-art research works have revealed the necessity of considering the transients of NGS in the optimal planning and scheduling operation of IGPS [29]–[34]. However, it is hard to analytically solve the partial differential equations (PDEs), which are the governing equations for transient analysis of NGS. To formulate a tractable optimization model for the scheduling operation of IGPS, different technologies (*e.g.*, *Wendroff* difference form and Euler finite difference form) have been adopted to transform the governing equations from PDEs into algebraic equations (AEs) for transient analysis of natural gas networks [29]–[35].

Moreover, the latest works [36]–[41] point out that the volatility of RES becomes a critical issue in power system operation because it results in the requirements of ramping capability rising. In practice, it has also been observed that the deviations from net loads (loads minus variable generations) or high rates of change beyond the visibility of the dispatch horizon could lead to the dispatchable resources with sufficient generation capacity, while without sufficient ramping capability to response the demand variations [42]. To handle the issue, the continuous-time generation and ramping trajectories are approximated with polynomials (*e.g.*, Hermite polynomials), and the day-ahead unit commitment model is reformulated in the function space in [43], [44].

Function space is spanned by an orthogonal function basis, such as polynomials, sine, and exponential functions. Optimization in function space is adopting the function basis to approximate time-variant trajectories under the desired error, mapping whole approximated trajectories into the function space and solving the related optimization problem through the coefficients of the function basis. Different from the optimization in algebraic space, the optimization in function space is mapping the time-variant trajectories on an interval of interest into the points in function space by projecting the trajectories to each function basis, rather than sampling them. The function space method has been successfully adopted to study electricity marketing clearing [45], transient stability [46], power flow [47]–[49], *etc*.

Motivated by the multi-time-scale characteristics of IGPS, the interdependence of tightly coupled IGPS, the high penetration of RES in the EPS section, and the novel idea about optimization in function space. Exploration is conducted to formulate a continuous spatial-temporal day-ahead optimal schedule model of IGPS in this paper. Firstly, the Bernstein polynomials are adopted to approximate the time-variant trajectories in EPS and spatial-temporal-variant trajectories in NGS. Then the operational matrices of differentiation and integration are developed to convert the governing equations representing the transient analysis of NGS from PDEs into AEs in Bernstein space. Finally, the proposed continuous spatial-temporal optimal schedule model of IGPS is formulated in Bernstein space, wherein the unit commitment model with DC power flow constraints for EPS and the dynamic gas flow model for NGS are adopted. The main **contributions** of this paper are summarized as follows:

1) ***New View***. It is a pioneering study to develop a continuous spatial-temporal day-ahead optimal schedule model of IGPS in the function space. The proposed model formulated

with the governing equations of NGS could be used for accurately scheduling the operation of IGPS when the transient process of NGS is considered.

2) ***New Approach***. It is an attempt to develop a resolution adaptive modeling method in the function space to formulate a continuous spatial-temporal optimal schedule model for IGPS. Different from the discretization, when the operational matrices, which are constant, are used for converting the PDEs (*i.e.*, the governing equations for transient process of energy transmission in NGS) into a set of AEs, the resolution limitations proposed in [34] do not need to be considered.

3) ***New Tool***. It is an exploration to set up a novel PDE constrained optimization for the energy management across multi-energy carriers, wherein the transient gas flow model and the unit commitment model with the static DC power flow constraints are reformulated in the function space.

The remainder of this paper is organized as follows, the Bernstein polynomials and the operational matrices in Bernstein space are introduced and developed in section II. Then, in section III, the day-ahead optimal schedule model of IGPS is formulated in the Bernstein space of order 3 (*i.e.*, $m = 3$) with considering the dynamics of energy transmission in NGS. Based on the case of a simple integrated system, section IV illustrates the comparison of numerical results to validate the formulated model, exhibit the necessity of considering the dynamics of NGS, and analyze the relationship between the response time of NGS and the parameters of pipelines. In section V, the simulation results of IEEE 39-bus EPS integrated with Belgian NGS demonstrate the effectiveness of the proposed optimal schedule model of IGPS in large systems. Additionally, the optimal scheduling operation problems of IGPS in the different scenarios of wind penetration and the roles of P2G facilities are analyzed by using the proposed continuous spatial-temporal optimal schedule model of IGPS. Finally, the conclusion is drawn in Section VI.

II. The Bernstein Polynomials and the Operational Matrices in Bernstein Space

The splines are effective tools to approximate a time-variant trajectory under an expected error by increasing the order of the spline basis [50]. There are various families of splines in the *Hilbert* space $\mathcal{H}$, thanks to many useful properties (*e.g.*, symmetry, convex hull, geometry invariance) of Bernstein polynomials [51], they are selected as the basis for splines in this paper, in other words, the Bernstein polynomials are adopted to develop the piecewise approximation of the sampling data sets on the whole interval of interest. In this section, firstly, the Bernstein polynomials will be briefly introduced, and the convex hull property of the Bernstein polynomials of order 3 will be exhibited. Then, the operational matrices of integration and differentiation will be introduced and developed, which are mathematical tools to transform the equations from PDEs to AEs.

A. Fundamental of the Bernstein Space

An mth-dimensional Bernstein space, *i.e.*, formulation (1), is built by combining $m+1$ Bernstein polynomials. In the mth-Bernstein space, each of the basis is positive, and the sum of all basis is equal to unity for all of variable $x \in [0,1]$, namely, $\sum_0^m B_i^m(x) = 1$.

$$B^m(x) = \begin{bmatrix} B_0^m(x) & B_1^m(x) & \cdots & B_m^m(x) \end{bmatrix}^{\mathrm{T}} \tag{1}$$

where the Bernstein polynomial of m-th degree defined on the interval $[0,1]$ is shown as follows [51].

$$B_i^m(x) = \binom{m}{i} x^i (1-x)^{m-i}, i \in [0,m], x \in [0,1] \tag{2}$$

A time-variant trajectory can be approximated in terms of a linear combination of Bernstein polynomials of order m, which is shown as (3), and the approximated curve is the so-called Béizer curve. Meanwhile, the time-variant trajectory could be represented by the coefficients $\mathbf{\Gamma^B}$ in Bernstein space of order m, if the Bernstein polynomials are regarded as the basis of a function space.

$$g(t) \simeq [B^m(t)]^{\mathrm{T}} \mathbf{\Gamma}^{\mathrm{B}},\ \mathbf{\Gamma}^{\mathrm{B}} \in \mathbb{R}^{m\times 1} \tag{3}$$

Similarly, a spatial-temporal surface can be approximated as (4), and the approximated surface is the so-called Bézier surface. And the coefficients $\mathbf{\Lambda^B}$ are the coordinate of the approximated surface in Bernstein space.

$$f(x,t) \simeq [B^m(x)]^{\mathrm{T}} \mathbf{\Lambda}^{\mathrm{B}} B^m(t),\ \mathbf{\Lambda}^{\mathrm{B}} \in \mathbb{R}^{m\times m} \tag{4}$$

The main motivation of adopting Bernstein polynomials is the convex hull property [51]. In other words, the curve (*e.g.*, generation and ramping trajectories) will always be inside of the convex envelopes (boundary) shaped by the coefficients of Bernstein polynomials, namely, the control points [51]. To make the convex hull property of Bernstein polynomials more clearly, an example of a hypothetical curve approximated by the Bernstein polynomials of order 3 is exhibited in Fig. 1. In the figure, the Bézier curve (*i.e.*, the black line) formed by Bernstein polynomials matches the hypothetical curve (*i.e.*, the red dash line). And the hypothetical curve is inside of the convex hulls shaped by the coefficients of Bernstein polynomials. Accordingly, it means the upper and lower limitations of the curve (*e.g.*, generation and ramping trajectories) in the τ-th interval can be respectively formulated by using the Bernstein coefficients.

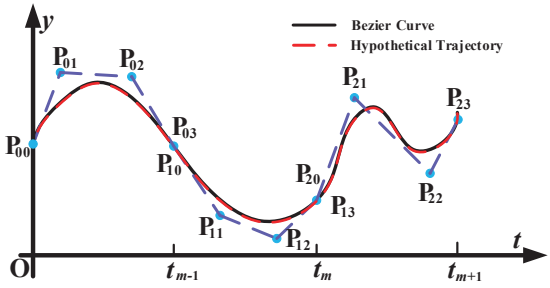

Fig. 1. The control points of Bernstein polynomials and the Bézier curve.

Similarly, for the surfaces (*e.g.*, mass flow rate and density), they will never be outside of the convex envelope surfaces formed by the control points (*i.e.*, elements of the matrix $\mathbf{\Lambda}^{\mathrm{B}}$

in Eq. 4) of Bernstein polynomials [51]. And the upper and lower limitations of the surface can also be respectively limited by the matrix elements of the Bernstein polynomials.

Note that the convex hull property of Bernstein polynomials provides a sufficient but unnecessary condition for properly bounding the upper/lower limits of the temporal/spatial-temporal function values over a finite dynamic range.

B. Operational Matrices in Bernstein Space

It is another considerable way to convert PDEs into AEs by using operational matrices to substitute for the operations (*i.e.*, integration and derivation) of PDEs in the function space [52], so that the optimal problems including PDE constraints are tractable. Motivated by the above way, the operational matrices are employed to transform the governing equations (*e.g.*, PDEs) for transient analysis of NGS into AEs in Bernstein space. The operational matrices of integration $\mathbf{I}$ and differentiation $\mathbf{D}$ have been developed in Bernstein space in [52], which are formulated in (5) and (6).

$$\int_0^x B^m(s)\mathrm{d}s \simeq \mathbf{I}B^m(x),\ x \in [0,1] \tag{5}$$

$$\frac{\mathrm{d}}{\mathrm{d}x}B^m(x) = \mathbf{D}B^m(x),\ x \in [0,1] \tag{6}$$

In order to convert the PDEs governing the dynamic characteristics of NGS into AEs in this paper, a new operational matrices of integration $\mathbf{K}$ on the interval $[x,1]$ is developed here, as shown in (7). The detailed derivation of the operational matrix of integration $\mathbf{K}$ is shown in Appendix-A.

$$\int_x^1 B^m(s)\mathrm{d}s \simeq \mathbf{K}B^m(x),\ x \in [0,1] \tag{7}$$

III. The Optimal Schedule Model of IGPS in Bernstein Space

In this section, the optimal schedule model of IGPS is formulated in Bernstein space, the degree $m = 3$. Firstly, the fundamental physical formulation (*i.e.*, the governing equations) for transient analysis of NGS is briefly introduced. Then, the optimal schedule model of IGPS is reformulated in Bernstein space. The main idea is to approximate the time-variant trajectory of EPS and the spatial-temporal variant trajectory of NGS by Bernstein polynomials, project the variant trajectories into Bernstein space, and reformulate the objective function and constraints of IGPS in Bernstein space.

A. Fluid Dynamics of Energy Transmission in NGS

The pressure along the pipeline drives the energy transmission in NGS. Assuming slow transients that do not excite waves and shocks [53], the one-dimensional spatial-temporal fluid dynamics of NGS are generally described using three major equations: the momentum equation (so-called Navier Stokes equation), the material balance equation and the state equation [54], which contain the gas states, *e.g.*, velocity, density, pressure. The Navier Stokes equation expresses the conservation of momentum for natural gas, the material balance equation describes the mass conservation of natural gas in the pipelines, and the state equation represents the relationship between density and pressure of natural gas.

Based on the assumptions, namely, the gas transmission is isothermal and the altitude change along the pipelines could be neglected [54], the governing equations of NGS are formulated as (8)-(10), where the variations x and t are not written for brevity.

$$\frac{\partial(\rho\omega)}{\partial t} + \frac{\partial p}{\partial x} + \frac{\lambda\rho\omega^2}{2d} = 0 \tag{8}$$

$$\frac{\partial\rho}{\partial t} + \frac{\partial(\rho\omega)}{\partial x} = 0 \tag{9}$$

$$p = c^2\rho \tag{10}$$

However, the deviatoric stress tensor term (*i.e.*, the third term) in the momentum equation (*i.e.*, Eq. (8)) is nonlinear. Our previous work (*i.e.*, Ref. [32]) has proven that it is an acceptable way that adopting average gas velocity $\bar{\omega}$ to linearize the nonlinear, so the nonlinear term can be approximated as:

$$\frac{\lambda\rho\omega^2}{2d} \simeq \frac{\bar{\omega}\lambda}{2d}\omega\rho \tag{11}$$

The mass flow rate M is defined as:

$$M = \rho\omega A \tag{12}$$

where the sign (flow direction) of M is up to the sign of ω, and the density ρ and the cross-sectional area of pipeline A will not influence the sign of M. Then, substituting the (11) and (12) into (8), the momentum equation is linearized as:

$$\frac{\partial M}{A\partial t} + \frac{\partial p}{\partial x} + \frac{\lambda\bar{\omega}}{2dA}M = 0 \tag{13}$$

Substituting the (12) into (9), the material balance equation can be reformulated as follow:

$$\frac{\partial\rho}{\partial t} + \frac{\partial M}{A\partial x} = 0 \tag{14}$$

Note that the (13), (14), and (10) will be adopted to represent the dynamics of natural gas networks in this paper.

B. The Continuous Spatial-Temporal Constraints of NGS

The governing equations (13), (14), and (10) for dynamic analysis of NGS are complicated to be directly adopted to describe the energy flow in the pipelines. In order to transform the PDEs (13) and (14) into AEs, which are tractable in optimization problems, a novel continuous spatial-temporal method originated from the function-space optimization is developed to deal with the PDEs by using operational matrices in Bernstein space, which is the **core** of this paper. The basic idea of the method is converting the PDEs into the equivalent integro-differential equations, which contain the boundary conditions of the PDEs. Then, the operational matrices are adopted to replace the operations of derivation and integration. As mentioned in Ref. [35], if any two of the boundary conditions $\rho(0,t)$, $\rho(1,t)$, $M(0,t)$ and $M(1,t)$ are initial conditions, the PDEs for dynamic analysis of energy transmission in NGS will be with a unique solution. For each of the gas pipeline, the variable MFR $M(x,t)$ and gas density

$\rho(x,t)$ can be expressed as (15), because there are observers at both ends of the pipeline.

$$\begin{aligned} M(x,t) &= M(1,t) - \int_x^1 \frac{\partial}{\partial s} M(s,t)\mathrm{d}s \\ \rho(x,t) &= \rho(0,t) + \int_0^x \frac{\partial}{\partial s} \rho(s,t)\mathrm{d}s \end{aligned} \tag{15}$$

Additionally, for each of the pipelines, the MFR $M(x,t)$ and gas density $\rho(x,t)$ also can be approximated by the Bernstein polynomials as (16).

$$\begin{aligned} M_{n,\tau}(x,t) &= \phi^T(x)\boldsymbol{M}_{n,\tau}\phi(t) \\ \rho_{n,\tau}(x,t) &= \phi^T(x)\boldsymbol{\rho}_{n,\tau}\phi(t) \end{aligned} \quad \forall n,t \tag{16}$$

where $\phi(x) = B^3(x)$ and $\phi(t) = B^3(t)$. At both ends of the pipeline, the observed gas density and MFR profiles are approximated with the Bernstein polynomials as equation (17).

$$\begin{aligned} M_{n,\tau}(1,t) &= \phi^T(x)\boldsymbol{M}_{n,\tau,0}\phi(t) \\ \rho_{n,\tau}(0,t) &= \phi^T(x)\boldsymbol{\rho}_{n,\tau,0}\phi(t) \end{aligned} \quad \forall n,t \tag{17}$$

Substituting (5)-(7), (13), (14), (16) and (17) into (15), the relationships between the MFR and gas density of each gas pipeline, *i.e.*, formulation (18), are obtained.

$$\begin{aligned} \phi^{\mathrm{T}}(x)\boldsymbol{M}_{n,\tau}\phi(t) &= \phi^{\mathrm{T}}(x)\left(\boldsymbol{M}_{n,\tau,0} + Al\mathbf{K}^{\mathrm{T}}\boldsymbol{\rho}_{n,\tau}\mathbf{D}\right)\phi(t) \\ \phi^{\mathrm{T}}(x)\boldsymbol{\rho}_{n,\tau}\phi(t) &= \phi^{\mathrm{T}}(x)\left(\boldsymbol{\rho}_{n,\tau,0} - \frac{l}{c^2A}\mathbf{I}^{\mathrm{T}}\boldsymbol{M}_{n,\tau}\mathbf{D}\right)\phi(t) \\ &\quad - \phi^{\mathrm{T}}(x)\left(\frac{\lambda\bar{\omega}l}{2dAc^2}\mathbf{I}^{\mathrm{T}}\boldsymbol{M}_{n,\tau}\right)\phi(t) \end{aligned} \tag{18}$$

In the light of the fact that the $\phi(x)$ and $\phi(t)$ are the Bernstein polynomials of distance and time respectively, and they are also the basis of the Bernstein space $\Theta \subset \mathcal{H}$. Hence, the equations (18) are expressed as equations (19) in Θ.

$$\begin{aligned} \boldsymbol{M}_{n,\tau} &= \boldsymbol{M}_{n,\tau,0} + Al\mathbf{K}^{\mathrm{T}}\boldsymbol{\rho}_{n,\tau}\mathbf{D} \\ \boldsymbol{\rho}_{n,\tau} &= \boldsymbol{\rho}_{n,\tau,0} - \frac{l}{c^2A}\mathbf{I}^{\mathrm{T}}\boldsymbol{M}_{n,\tau}\mathbf{D} - \frac{\lambda\bar{\omega}l}{2dAc^2}\mathbf{I}^{T}\boldsymbol{M}_{n,\tau} \end{aligned} \tag{19}$$

where all of the elements in equations (19) are not related to the variables of time and distance (*i.e.*, t and x) anymore. Therefore, the PDEs for transient analysis of NGS are successfully converted into a set of AEs in the Bernstein space. The authors have to emphasize that due to the definition domain of Bernstein polynomials are on the interval $[0,1]$, the length of the pipeline and the time horizon of interest must be scaled into the definition domain, respectively, and the scale factors (*e.g.*, the length l) will arise in Eq. (18) and (19).

Furthermore, in natural gas networks, the source nodes are with constant pressure conditions, and the sink nodes fulfill the demand of consumers, including the fuels of GFUs. Besides, the gas demands at sink nodes and the gas pressure at source nodes are formulated as (20) and (21) in Θ, respectively.

$$M_{load_{n,\tau}}(t) = \phi^{\mathrm{T}}(x)\boldsymbol{M}^D_{n,\tau}\phi(t) \tag{20}$$

$$\rho_{source_{n,\tau}}(t) = \phi^{\mathrm{T}}(x)\boldsymbol{\rho}^S_{n,\tau}\phi(t) \tag{21}$$

Hence, the equality constraints at the source or sink nodes of natural gas networks are represented as formulations (22) and (23), respectively.

$$\boldsymbol{\rho}_{n,\tau,0} = \boldsymbol{\rho}^S_{n,\tau}, \quad \forall n \in \{source\ node\} \tag{22}$$

$$\boldsymbol{M}_{n,\tau,0} = \boldsymbol{M}^D_{n,\tau}, \quad \forall n \in \{sink\ node\} \tag{23}$$

In the junctions, the gas pressure and density of different pipelines should be consistent. According to the law of mass conservation, the mass flux injection (positive) and withdrawal (negative) of each pipeline should keep a balance at the intersections. The constraints in (24) enforce the aforementioned nodal conditions at the intersection in Θ.

$$\begin{aligned} &\phi^{\mathrm{T}}(x_i)\boldsymbol{\rho}_{n_1,\tau} = \phi^{\mathrm{T}}(x_j)\boldsymbol{\rho}_{n_2,\tau} = \cdots = \phi^{\mathrm{T}}(x_n)\boldsymbol{\rho}_{n,\tau} \\ &\phi^{\mathrm{T}}(x_i)\boldsymbol{M}_{n_1,\tau} + \phi^{\mathrm{T}}(x_j)\boldsymbol{M}_{n_2,\tau} + \cdots + \phi^{\mathrm{T}}(x_n)\boldsymbol{M}_{n,\tau} = 0 \\ &where \quad x_i, x_j, \cdots, x_n = \{x | x = 0\ or\ 1\} \end{aligned} \tag{24}$$

In practice, the density and MFR should not exceed the operation boundaries (upper and lower) of the pipelines. In light of the convex hull property of Bernstein polynomial [51], the constraints could be formulated as (25) in Θ.

$$\begin{aligned} max(|\boldsymbol{M}_{n,\tau}|) &\le \overline{M_n} \\ max(|\boldsymbol{\rho}_{n,\tau}|) &\le \overline{\rho_n} \end{aligned} \quad \forall n,t \tag{25}$$

As discussed before, the constraints in (19) govern the fluid dynamics in pipelines of NGS, the nodal condition constraints at source nodes, sink nodes and intersections are formulated as (22) - (24), and the constraints in (25) enforce the states of each pipeline within operation boundaries in Θ.

C. The Continuous Time Constraints of EPS

At the power system side, the day-ahead UC problem is embedded in the optimal schedule model. In Bernstein space, the day-ahead continuous time-variant load and generation trajectories are approximated by (26) and (27), respectively.

$$\hat{L}_{m,\tau}(t) \simeq [B^3(t)]^{\mathrm{T}}\mathbf{L}_{m,\tau} \tag{26}$$

$$\hat{G}_{k,\tau}(t) \simeq [B^3(t)]^{\mathrm{T}}\mathbf{G}_{k,\tau} \tag{27}$$

Based on the piecewise linear approximation of generation cost [55], the capacity range of the kth generation from $\underline{G}_k$ to $\overline{G}_k$ is divided to N_k parts. So the variables $\mathbf{H_{k,t,m}} = [H^1_{k,t,m}\ H^2_{k,t,m}\ H^3_{k,t,m}\ H^4_{k,t,m}]^{\mathrm{T}}, \forall m = \{1,2,3,\cdots,N_k\}$ are used to represent the schedule on the mth linear section. The real generation schedule can be expressed as follow:

$$\mathbf{G}_{k,\tau} = \underline{G}_k\mathbf{I}_{k,\tau} + \sum_{m=1}^{N_k}\mathbf{H}_{k,\tau,m} \tag{28}$$

According to the operational matrix of derivation in Bernstein space, the continuous time-variant ramping trajectory of generation units can be represented as (29).

$$\frac{\mathrm{d}}{\mathrm{d}t}\hat{G}_{k,\tau}(t) = [B^3(t)]^{\mathrm{T}}\mathbf{D}^{\mathrm{T}}\mathbf{G}_{k,\tau} = [B^3(t)]^{\mathrm{T}}\dot{\mathbf{G}}_{k,\tau} \tag{29}$$

where $\dot{\mathbf{G}}_{k,\tau} = [\dot{G}^1_{k,\tau}\ \dot{G}^2_{k,\tau}\ \dot{G}^3_{k,\tau}\ \dot{G}^4_{k,\tau}]^{\mathrm{T}}$ is the coefficients of the ramping trajectory of the kth unit on the interval $[t, t+1]$.

The Ref. [43] has already formulated the constraints of power balance, generation continuity, generation capacity, and ramping in the function space. Similarly, the constraints of nodal active power balance (30), generation continuity (31),

generation capacity (32), generation ramping (33)-(36), and DC power flow constraints (37)-(38) on the τ-th interval, (*i.e.*, $[t, t+1]$) are also developed in Bernstein-based function space. For the continuous-time linear DC power flow constraint, the active power flowing in the transmission line is constrained by the thermal limits of the transmission capacity as (38).

$$\sum_{k\in N_b}\mathbf{G}_{k,\tau}+\sum_{m\in N_b}\mathbf{L}_{m,\tau}+\sum_{i\in N_b}\mathbf{P}_{ij,\tau}+\sum_{k\in N_b}\mathbf{G}^{RES}_{k,\tau}=0 \tag{30}$$

$$G^1_{k,\tau+1}=G^4_{k,\tau},\dot{G}^1_{k,\tau+1}=\dot{G}^4_{k,\tau} \tag{31}$$

$$\underline{G}_k\mathbf{I}_{k,\tau}\le\mathbf{G}_{k,\tau}\le\overline{G}_k\mathbf{I}_{k,\tau} \tag{32}$$

$$\dot{G}^1_{k,\tau}\le R^U_k 1_{k,\tau}+R^{SU}_k[1_{k,\tau}-1_{k,\tau-1}]+\overline{G}_k[1-1_{k,\tau}] \tag{33}$$

$$-\dot{G}^1_{k,\tau}\le R^D_i 1_{k,\tau}+R^{SD}_k[1_{k,\tau-1}-1_{k,\tau}]+\overline{G}_k[1-1_{k,\tau-1}] \tag{34}$$

$$[\dot{G}^2_{k,\tau}\ \dot{G}^3_{k,\tau}]\le R^U_k[1_{k,\tau}\ 1_{k,\tau}]+\overline{G}_k[1-I_{k,\tau}\ 1-I_{k,\tau}] \tag{35}$$

$$[-\dot{G}^2_{k,\tau}\ -\dot{G}^3_{k,\tau}]\le R^D_k[1_{k,\tau}\ 1_{k,\tau}]+\overline{G}_k[1-1_{k,\tau}\ 1-1_{k,\tau}] \tag{36}$$

$$\mathbf{P}_{ij,\tau}=\frac{1}{X_{ij}}(\boldsymbol{\theta}_{i,\tau}-\boldsymbol{\theta}_{j,\tau}) \tag{37}$$

$$max(|\mathbf{P}_{ij,\tau}|)\le\overline{P}_{ij} \tag{38}$$

D. The Formulation of Energy Conversion in Bernstein Space

There are two kinds of facilities (*i.e.*, P2Gs and GFUs) as interfaces between electricity and natural gas, so the EPS and NGS are bi-directionally coupled with each other. The P2G facilities consume electrical power to produce natural gas. On the contrary, GFUs consume natural gas fuels to generate electricity. In Bernstein space Θ, the P2G facilities are formulated as (39).

$$\boldsymbol{M}_{n,\tau,0}=\eta^p_{n,i}\boldsymbol{L}_{i,\tau}\quad\forall(n,i)\in\{\text{P2G }node\} \tag{39}$$

where the subscript (n,i) indicates the P2G facility connected to Bus i at the EPS side creates the natural gas injected to the Node n. Meanwhile, the energy conversion of GFUs is mathematically represented as follow:

$$\boldsymbol{G}_{k,\tau}=\eta^g_{k,n}\boldsymbol{M}_{n,\tau,0}\quad\forall(n,k)\in\{\text{GFU }node\} \tag{40}$$

where the subscript (k,n) indicates natural gas fuel at the Node n of NGS is consumed to generate electricity at the Bus k of EPS by the GFUs. The unit of $\eta^p_{i,k}$ is $\mathrm{kg/(s\cdot MW)}$, and the unit of $\eta^g_{k,i}$ is $\mathrm{MW\cdot s/kg}$.

E. The Objective Function of IGPS in Bernstein Space

For the day-ahead optimal schedule model of IGPS, the objective is to minimize the total generations cost J^{ps}_{cost} plus the gas consumption J^{gs}_{cost} on both the day-ahead schedule interval Ω_{ps} of EPS and the schedule area Ω_{gs} of NGS (*i.e.*, minimizing the total energy consumption), which is shown as (41). The generation cost at the EPS side is linearized to approximate the quadratic cost function of generation [55]. The capacity range of the kth generation from minimum to maximum is separated into N_k parts, and the cost coefficients of the m-th part are $\alpha_{k,m},\forall m=\{1,2,\cdots,N_k\}$

F. The Summary of Optimal Schedule Model of IGPS

Based on those mentioned above, the continuous spatial-temporal optimal schedule model of IGPS in Bernstein space Θ is summarized as follows:

Objective function: formulation (41).

Subject to: a. Power System Constraints: (30) - (38).
b. Gas System Constraints: (19) and (22) - (25).
c. Energy Conversion Constraints: (39) and (40).

In the objective function, the cost coefficients are configured according to the realistic price. In the NGS, a positive cost coefficient of natural gas is set to minimize the gas fuel consumption. In the EPS, the cost coefficient of wind turbines is set as the lowest one to maximize the accommodation of wind energy, a positive cost coefficient of GFU is configured to minimize the fossil fuel consumption, which is higher than the natural gas's under the condition of the same energy. Moreover, it is evident that the optimal schedule model of IGPS is a MILP problem in Bernstein space. Hence, it can be solved using commercial MILP solvers (*e.g.*, Cplex, Gurobi).

As the convex hull property of Bernstein polynomials, which is one of the fundamentals that the presented approach bases on, provides a sufficient but unnecessary condition for formulating the upper/lower limit constraints of the temporal/spatial-temporal waveforms, the proposed modeling approach may be conservative.

IV. Case I: A Simple IGPS

In this section, the numerical results for a case study are based on a pipeline segment and a simple IGPS, respectively. Firstly, the formulated dynamic gas flow model of NGS in Bernstein space is validated by comparing the simulation results of the proposed model and the differencing model from Ref. [32]. Then, this study case is also used to reveal the significant difference between the transient model and the steady-state model of NGS. Afterwards, the relationship between the parameters (*i.e.*, length and diameter) of pipelines and the time constant of NGS is investigated. Finally, a simple integrated gas and power system demonstrates the reason for adopting the dynamic model of NGS.

A. Model Validation

The case of a single pipeline is shown in fig. 2, the length and diameter of the single pipeline are $100\ \mathrm{km}$ and $0.9\ \mathrm{m}$, respectively. The left end is source node and the right end is sink node. The pressure is set to $6\ \mathrm{MPa}$ constantly at the source node and the gas demand at the sink node is shown as the red curve in fig. 3(a). The formulation from the proposed continuous spatial-temporal model and the differencing model

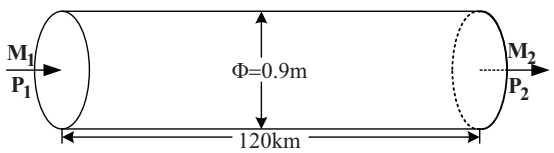

Fig. 2. A single pipeline.

$$
\begin{aligned}
min\left(J_{cost}^{ps}+J_{cost}^{gs}\right) &= min\left(\int_{\Omega_{ps}} C_{ps}(\mathbf{G},\mathbf{I})\mathrm{d}t+\int_{\Omega_{gs}} C_{gs}(\mathbf{M},\boldsymbol{\rho})\mathrm{d}t\right)\\
&= min\sum_{k=1}^{N_g}\sum_{\tau=0}^{T_N}\left\{\overline{C_{k,\tau}}+\underline{C_{k,\tau}}+\left[c_{k,\tau}\cdot 1_{k,\tau}+\sum_{m=1}^{N_k}\left(\frac{\alpha_{k,m}}{4}\sum_{i=0}^{3}H_{k,\tau,m}^{i}\right)\right]\right\}+\sum_{s=1}^{N_S}\sum_{\tau=0}^{T_N}\left(\frac{\beta_{s,\tau}}{4}\sum_{i=0}^{3}M_{s,\tau}^{1,i}\right)
\end{aligned}
\tag{41}
$$

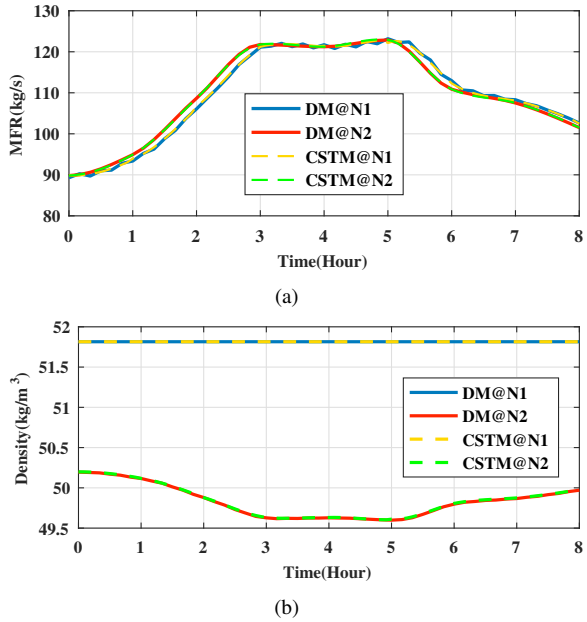

Fig. 3. Comparative simulations between the proposed continuous spatial-temporal model (CSTM) and differencing model (DM). (a) The MFR at both ends of the single pipeline using the proposed model and differencing model. (b) The nodal pressure of the single pipeline using the proposed model and differencing model.

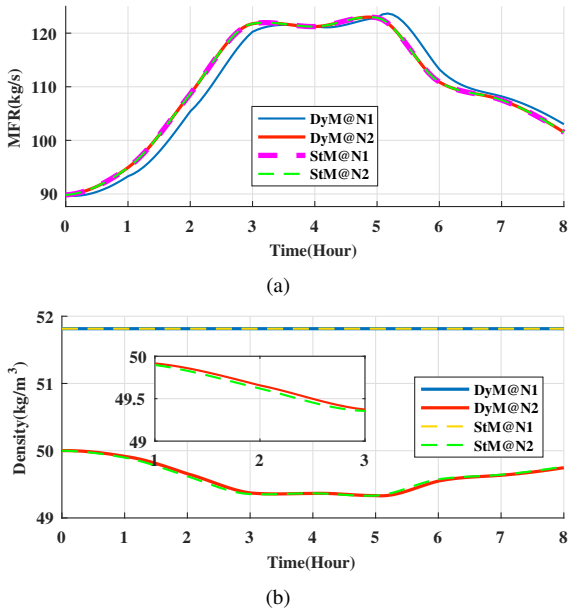

Fig. 4. Comparison between the static model (StM) and dynamic model (DyM) of gas flow. (a) The nodal MFR of the single pipeline with the static and dynamic model. (b) The nodal density of the single pipeline with the static and dynamic model.

have been solved by Matlab. The dynamic simulation results of the proposed model and differencing model, illustrated in fig. 3, demonstrate the gas diffusion process in the pipeline is the same when both models are simulated, *i.e.*, the pressure of the pipeline increases, when the injection mass flow is higher than the withdrawal mass flow, and vice versa. Therefore, the proposed model is validated to accurately express the dynamic characteristics of energy transmission in the pipeline.

B. Comparison Between Static and Dynamic Gas Model

To investigate the effect brought by the dynamics of energy transmission in the pipe, the static and dynamic models are compared. To fair comparison, the terms respected to time t in the PDEs (13) and (14) are omitted. Then, the same scheme, for example, using integro-differential equations and operational matrices, is adopted to develop the static model in Bernstein space. Meanwhile, the other constraints of the IGPS remain the same. The simulation results of the two models are shown in fig. 4. The results show that the MFR and gas pressure in a pipeline with two different models. Fig. 4(a) indicates that due to the neglect of the term $\frac{\partial M}{\partial x}$ of Eq. 13 in the static model, the MFR always keeps the same along the whole pipeline, which could not accurately represent the physical transient process of the gas flow in the NGS. Different from the static model, the MFR at the left end (*i.e.*, source node) lags the right end (*i.e.*, load node) when the dynamic model is adopted, which is the same as the physical transient phenomenon of the gas flow in the NGS. The fig. 4(b), for the density (or pressure) along the entire pipeline segment, demonstrates the density difference between two ends of the pipeline from the static model is a little bit greater than the value from the dynamic model while the gas demands rise, and vice versa. The results are caused by neglecting the influence of the term $\frac{\partial \rho}{\partial t}$.

C. The Relationship Between the Response Time of NGS and the Physical Parameters of Pipeline

In this subsection, the pipelines varied with their own length and diameter are employed to study the relationship between the response time of NGS and the physical parameters of the pipeline. They are divided into two groups, one is with a constant diameter $(0.9m)$ and diversified length $(90km, 70km, 50km)$, the other group is with a constant length $(60km)$ and diversified diameter $(0.9m, 0.5m, 0.3m)$. To fair comparison, other physical conditions of the pipelines and the boundary conditions of the NGS remain the same in the numerical calculations. The numerical results of the pipelines are exhibited in fig. 5. The figures reveal that the response time of the NGS is related to the parameters (*i.e.*, length and diameter) of pipelines. Furthermore, it can be observed from fig. 5(a) that if the length of the pipeline is

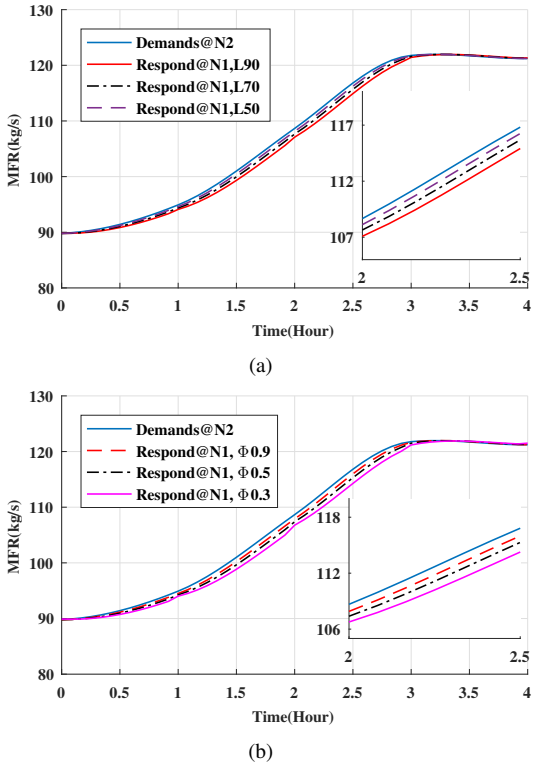

Fig. 5. The relationship between the response time of NGS and the physical parameters of the pipeline. (a) The response time is affected by the length of pipelines. (b) The response time is affected by the diameter of pipelines.

longer, the change of load demands will take more time to spread to the source node of NGS, namely, the response time of NGS is longer, and vice versa. Fig. 5(b) demonstrates that if the diameter of the pipeline is larger, the response time of the NGS will be shorter, and vice versa.

D. The Analysis of A Simple IGPS

A simple integrated gas and power system (shown in Fig. 6) comprising a gas-fired generator, a transmission line, a gas source, a pipeline, a gas load, and an electric load is selected as the test system. For the test system, the dynamic and static models of NGS are respectively cooperated with the UC model to evaluate the energy (gas fuel) cost. In both cases, the electric load, gas load, and total gas demand profiles are illustrated as the blue, red, and green curves in Fig. 7, respectively. Besides, we assumed that the price of natural gas is segmented, which is listed in Tab. I.

TABLE I
THE SEGMENTED PRICE OF GAS FUEL

Time	0:00 - 8:00	8:00 - 18:00	18:00 - 24:00
Price($/kg)	0.26	0.65	0.31

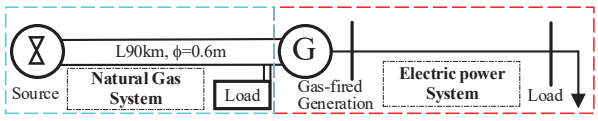

Fig. 6. A simple integrated gas and power system.

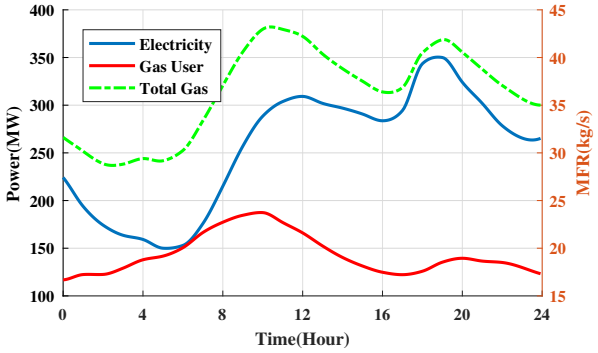

Fig. 7. The demands of electricity, gas user and total gas.

TABLE II
THE TOTAL COST OF GAS FUEL

Model	dynamic model	static model
Cost of gas fuel($)	974,021.68	974,680.22

The total costs of gas fuel with both models are summarized in Tab. II. In Tab. II, the total cost of gas fuel with the dynamic model is $\$974,021.68$, while the total cost of gas fuel with the static model is $\$974,680.22$. Compared with the static model, the dynamic model results in a cost reduction of $\$658.54$. In other words, the optimal schedule using the static model of NGS would be more costly. Since the static model does not take into account the linepack capability of pipeline and the slower moving speed of gas flow, the simulation results of the static model may be impractical and suboptimal. On the other hand, it can be observed that the gas-fired unit is one of the essential consumers, and the larger swings (up and down) of gas demands have occurred because of the fluctuations of electric load in Fig. 7. With the changing of demand, the gas flow in pipeline is fluctuating. For this situation, the linepack (*i.e.*, the volume of gas stored in pipe) plays a critical role that affects the ability to supply natural gas to the consumers. In order to satisfy the demands of GFUs and other gas loads within a reasonable pressure range, the natural gas network would have to manage the linepack. However, the linepack equation derived from the static model of NGS cannot accurately calculate the volume of gas stored in the pipe under dynamic situations [29]. Consequently, it is necessary to calculate the volume of natural gas stored in pipeline using the dynamic model. Meanwhile, it is essential to evaluate the grade of flexibility and reliability that power systems require from gas systems with the dynamic model involving the compressibility, slower velocity, and longer stabilization times of NGS.

V. CASE II: A LARGE-SCALE IGPS

In this section, with the aim of demonstrating the effectiveness of the proposed continuous spatial-temporal optimal schedule model of IGPS in large systems, all numerical simulations are based on the combination of the IEEE 39-bus EPS and Belgian NGS [56]. Then, the analysis in the scenarios with different penetration of wind energy is conducted. Finally, the role of P2G on the improvement of wind accommodation is evaluated.

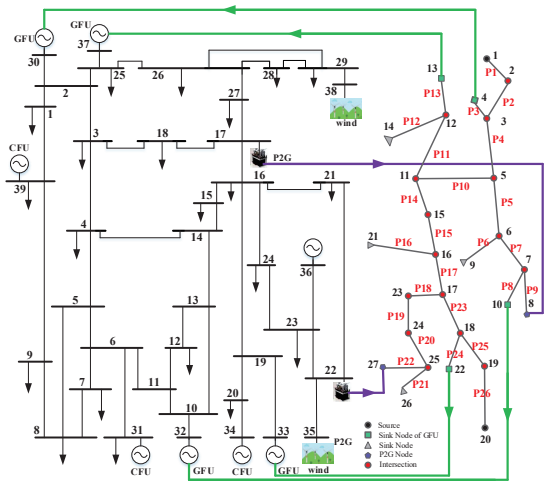

Fig. 8. The integrated gas and power energy testing system.

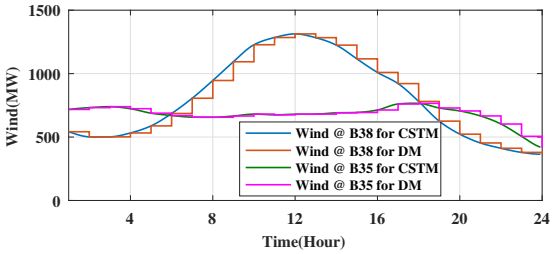

Fig. 9. The wind farm profiles at Bus 35 and Bus 38 of the continuous spatial-temporal model (CSTM) and differencing model (DM).

A. Outline of the Testing IGPS

The IEEE 39-bus EPS and Belgian NGS [56] is integrated as a test system of IGPS, which is shown in fig. 8. In the EPS, the wind farms are placed at the Bus 35 and 38, the P2G facilities are installed at the Bus 17 and 22, and the generation plants at Bus 30, 32, 33 and 37 are equipped with GFUs. The NGS contains two source nodes (Node 1 and 20), two P2G nodes (Node 27 and 8), four GFU connected nodes (Node 4, 10, 13, and 22), and four other sink nodes. Besides, the capacities of P2Gs are 100MW and 200MW, respectively.

The primary data of the IGPS are from practical historical operation data of Danish EPS and NGS [57], and they are scaled down to match the capacities in the studied system. Fig. 9 illustrated the wind profiles at Bus 35 and Bus 38 of the EPS, wherein the total wind power output is in the range from 787.9 to 1954.7 MW, the penetration of wind power in the EPS reaches 48.55%, and the scale factors of the wind farm are 0.237 and 0.303, respectively. The factor 0.26 is used to scale the electricity demand profiles, and the aggregated electricity demand is in the range from 2206.7 to 3744.9 MW. The natural gas load profiles are scaled by the factor 0.21, and full gas demand expecting GFUs is in the range from 204.9 to 294.8 kg/s.

B. Performance Analysis of the Proposed Model

1) *The computational efficiency of the proposed model and the differencing model.* The study case formulated by the proposed continuous spatial-temporal model and the Lax-Wendroff differencing model [32] is solved by using Cplex 12.8.0 on the laptop computer with an Intel Core-i5 processor @ 2.30 GHz and 8 GB of RAM. The proposed continuous spatial-temporal model averagely takes 106.83 seconds, and the Lax-Wendroff differencing model averagely consumes 24.93 seconds. Although the computational time of the proposed model is longer than the differencing model's, the proposed model not only takes into account the sampling points at both ends of the interval of interest, which is done in the differencing model, but also considers the trajectories (and surfaces) on the interval of interest. Hence, the more detailed operating information of IGPS is taken into consideration in the proposed model.

2) *The energy consumption analysis of IGPS.* The optimal energy consumption results of the study case in the 24-hour time horizon are illustrated in fig. 10. At the power system side, fig. 10(a) demonstrates the optimized operation schedule of the generation units with the high integration of wind energy. The ten generation units are divided into three groups (*i.e.*, GFUs, CFUs, and wind generation units) in different colors (*i.e.*, blue, green, and yellow). The generation trajectories indicate that the wind generation units supply almost half of the electricity demand (48.55%), 14.34% of electricity is produced by the GFUs, which is considerable. And the rest of the electricity (37.11%) is from the CFUs. Additionally, the figure indicates the generation units efficiently respond to the variation of the electric load demand (*i.e.*, the red line).

At the gas system side, fig. 10(b) demonstrates the optimal MFR at two source nodes and the optimal scheduling of the P2G facilities for the whole day. Due to the limited capacity of the P2G stations, only 0.68% of natural gas is produced by electrolysis, and 99.32% of the gas demand is supplied by the source nodes.

3) *The performance analysis of the transient in the NGS.* In order to visualize the dynamic characteristics of energy flow in the pipelines of NGS, a part of the numerical results

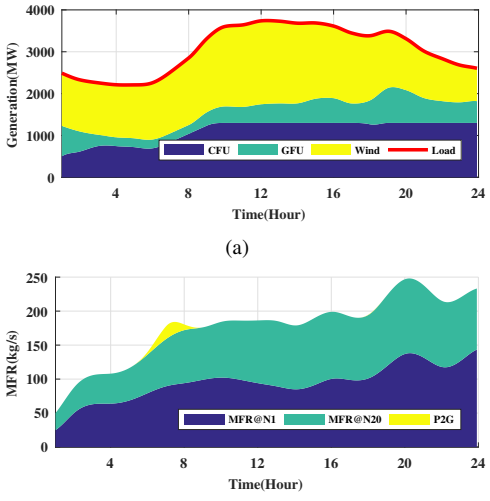

Fig. 10. Optimal schedule of IGPS. (a) Optimal generation schedule. (b) Optimal gas system schedule.

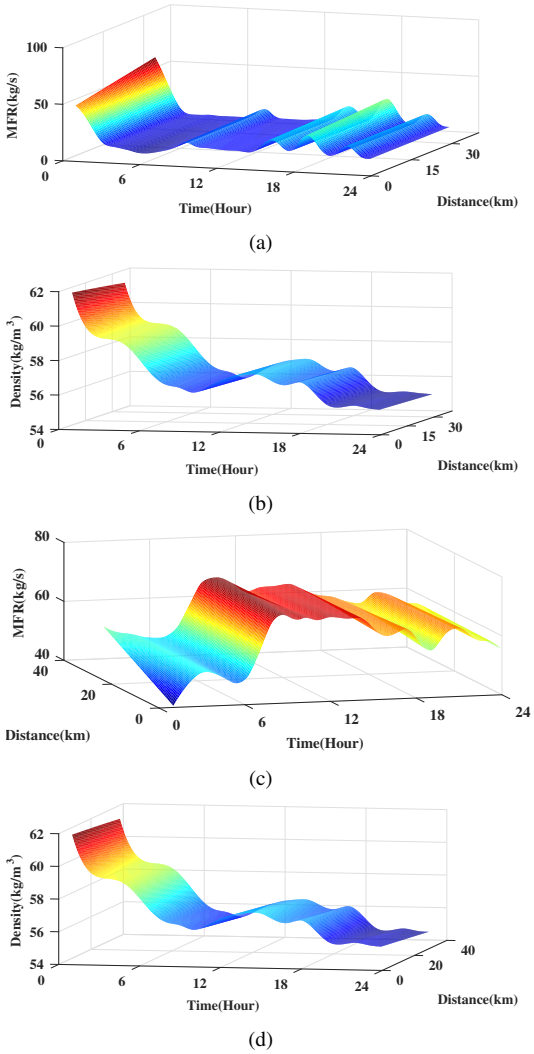

Fig. 11. The dynamic performance of IGPS in the spatial-temporal coordinate system. (a) The distribution of MFR of pipeline 12-13. (b) The distribution of density of pipeline 12-13. (c) The distribution of MFR of pipeline 12-14. (d) The distribution of density of pipeline 12-14.

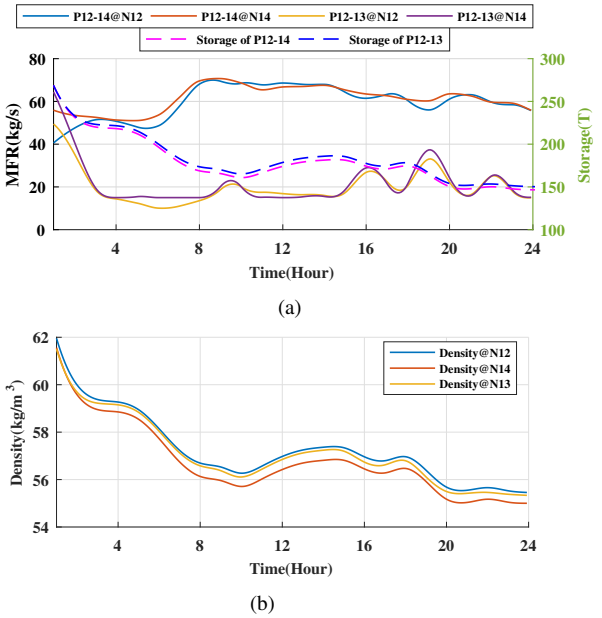

Fig. 12. The dynamic performance of IGPS. (a) The MFR at each end of the pipeline 12-13 and pipeline 12-14, and the storage in both pipelines. (b) The density at each end of the pipeline 12-13 and pipeline 12-14.

about the transient in the NGS by the proposed model is exhibited. Fig. 11 has represented the MFR and density transient processes of the pipeline 12-13 (*i.e.*, P13) and the pipeline 12-14 (*i.e.*, P12) by the surfaces in a spatial-temporal coordinate system, respectively. Fig. 12 has demonstrated the MFR and density dynamic processes at Node 12, Node 13 and Node 14 by the curves in a continuous time coordinate system, respectively. The whole spatial-temporal transient process of energy delivery in both of the pipelines can be clearly observed in fig. 11. The figures about the transient process of the energy transmission have revealed that (a) The change of the demands (*e.g.*, GFU and consumer demands) "spread" from one end to the other end of the pipeline with visible time. In other words, the change of the states (*i.e.*, MFR and density) at the Node 12 lags the states change at the Node 13 and Node 14. (b) If the MFR at Node 12 is greater than the MFR at the Node 13 (or 14), the density of the pipeline will increases, and vice versa. (c) If the MFR in the pipeline rises, the difference in density between both ends of the pipeline will be larger, and vice versa. (d) Due to the connection at Node 12, the states of both pipelines are not only affected by the change of its own load demands, but they have also been impacted by the state's change of the connected pipeline.

4) *The analysis of the natural gas storage in the pipeline.* Due to the compressibility of natural gas, the pipeline has the capacity to store natural gas by increasing the density (or pressure) of the pipelines. The gas storage $S_{ij}^g(t)$ in the pipeline ij can be assessed as follow:

$$S_{ij}^g(t) = S_{ij}^g(t_0) + \int_{t_0}^{t} (M_{ij}(0,\tau) - M_{ij}(L,\tau))\mathrm{d}\tau \qquad (42)$$

where $S_{ij}^g(t_0)$ indicates the amount of natural gas in the pipeline at t_0. $M_{ij}(0,\tau)$ and $M_{ij}(L,\tau)$ are the MFR at two ends of the pipeline ij, respectively.

According to Eq. (42) and the storage of each pipeline segment at $t = 0$, the linepack storage in the pipeline 12-13 and pipeline 12-14 are illustrated as the blue and purple dashed curve in fig. 12(a), respectively. From the fig. 12, it is clearly observed that the density (or pressure) and gas storage volume in the pipeline segment increases, if the injection gas volume is higher than the withdrawal gas volume, and vice versa. Thanks to the linepack storage in the pipeline, the gas network can quickly follow the fast variation of the natural gas demands at Node 13 and Node 14.

Furthermore, fig. 13(a) demonstrates that the storage of each pipeline at the end of every hour during the whole day, and fig. 13(b) and 13(c) show the storage of each pipeline at $t = 1$ and $t = 24$, respectively, wherein the related number of the pipelines in the bar figures are labeled with red letters in fig. 8. The bar figures indicate that the storage amount of each pipeline varies with time, and the gas storage of each pipeline in the whole network is almost different in each hour. The variance of gas storage in each pipeline is caused by the

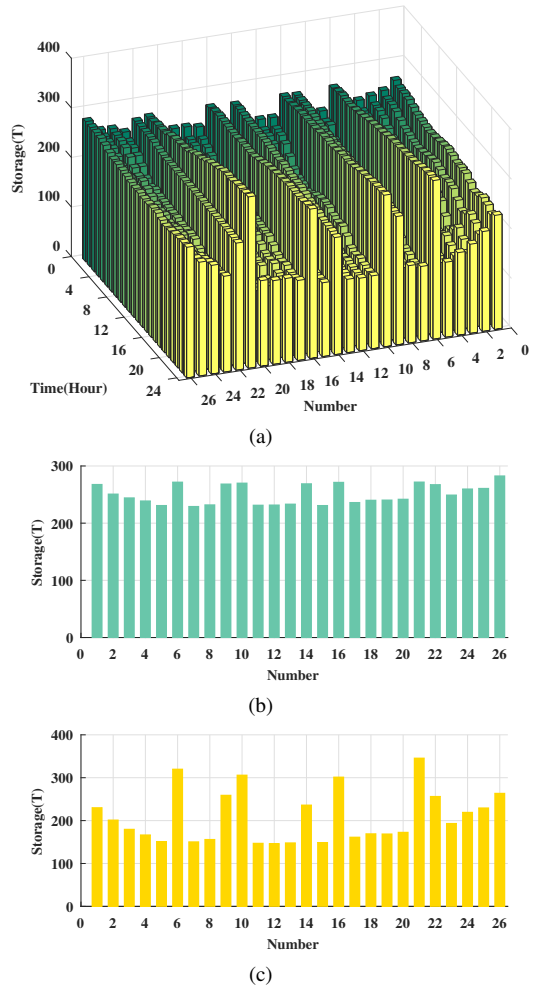

Fig. 13. The line-pack storage in the gas networks. (a) The line-pack storage of each pipeline at every hour during the whole day. (b) The line-pack storage of each pipeline at 1:00. (c) The line-pack storage of each pipeline at 24:00.

various demands at each sink node, including the demands of the GFUs. It exhibits that gas storage in gas networks plays a vital role in balancing the gas supplies and demands timely.

C. Evaluation of the Role of P2G

The power to gas facilities are emerging in EPS recently, they mainly play a role as an electricity consumer (*i.e.*, electric load). In this subsection, the role of P2G on the improvement of wind accommodation is evaluated. Fig. 14(a) demonstrates the IGPS simulation results when none of a P2G facility is installed, and the other operating conditions remain unchanged. In this scenario, as the electricity generation is greater than the demand of the loads in EPS, there is surplus wind energy during hours 5 to 9, but there are no P2G facilities, so the system operators only could curtail the surplus wind energy. Compared with the previous scenario, shown in fig. 14(b), all of the surplus wind energy is consumed by the installed P2G to produce natural gas. Although it is not an extremely high-efficiency way using electricity to produce natural gas, it is one of the most economical and reliable energy storage ways that storing the natural gas produced by surplus wind energy in the pipelines of NGS.

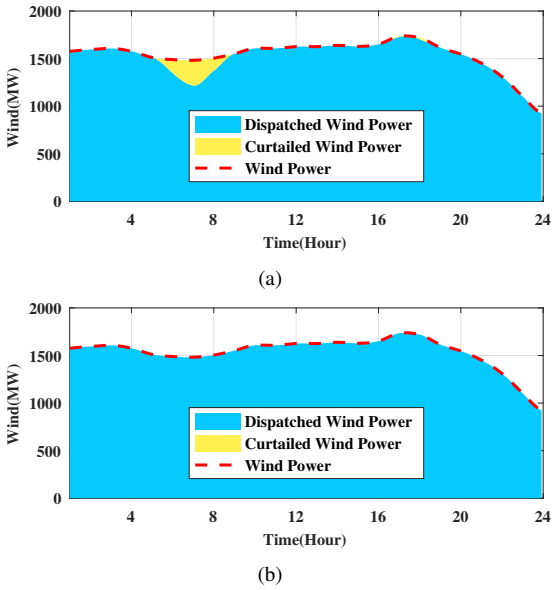

Fig. 14. Wind power accommodation. (a) P2G facilities are uninstalled in the IGPS. (b) P2G facilities are installed in the IGPS.

TABLE III
THE POWER CONSUMPTION BY P2G

	Wind Energy Penetration (%)	Surplus Wind Energy (MWh)	Power Consumed by P2G (MWh)
Case 1	25	16.23	16.23
Case 2	50	83.72	83.72
Case 3	60	234.15	234.15
Case 4	75	2236.91	1969.13
Case 5	85	3959.18	2286.46
Case 6	90	5027.60	2359.67

Additionally, the cases of different wind power penetration (*i.e.*, the fraction of total energy generated by wind turbines respected to the amount of generation) are also calculated by scaling the deterministic wind power profiles with different scale factors. The numerical results of the cases are listed in Tab. III. The electricity consumption results of P2G in the table indicate that the electric loads will rise so that the more wind energy could be accommodated when the energy delivery is not limited (*e.g.*, limited by the capacity of transmission line) in the EPS, because the P2G facilities consume the electricity to produce natural gas (or hydrogen) by the electrolysis, and the produced natural gas (or hydrogen) could be stored in the pipelines of NGS. At the same time, the Tab. III also reveals that the total surplus wind energy is dispatched to create natural gas (or hydrogen) through P2G when the wind energy penetration or the surplus wind energy is small, and the power of the surplus wind energy is below 300 MW. However, with the increasing penetration of wind energy, the power of surplus wind energy is beyond the limitation of the P2G capacity (300 MW), the excess part of the surplus wind energy still is curtailed. The cases have been demonstrated the good performance of the proposed model.

VI. CONCLUSION

This paper presents a continuous spatial-temporal optimal schedule model for the integrated gas and power system. The

optimization problem of IGPS is formulated in the function space, rather than the conventional algebraic space. The Bernstein functions of order 3 are adopted to reformulate the governing equation of NGS, namely, the partial differential equation constraints. The comparative simulation in a single pipeline validates the proposed model with the governing equation (*i.e.*, the Navier-Stokes equations) is capable of the transient analysis of NGS. Furthermore, the proposed model can quantify the variation of the linepack storage in each pipeline of NGS. In the study cases of IGPS, the simulation results demonstrate the proposed continuous spatial-temporal optimal schedule model of IGPS with considering the dynamics of NGS works well and efficiently in the different wind energy penetration scenarios and the P2G facilities are beneficial to promote wind energy accommodation in the IGPS. Moreover, compared with the Lax-Wendroff differencing model, although the proposed model would take more computational time in the study case, the average computational time (*i.e.*, $106.83s$) is still acceptable. Therefore, the proposed continuous spatial-temporal optimal schedule model of IGPS has the potential to be used for a practical bulk integrated natural gas and power system. The future works will formulate a continuous spatial-temporal optimal schedule model of IGPS, which will include the transient of compressors constraints, the constraints of AC power flow equations, or the constraints of DC power flow embedded the power losses.

ACKNOWLEDGEMENTS

The first author would like to thank the China Scholarship Council (CSC), Beijing, China, for econimic support of visiting the Aalborg University, Aalborg East, Denmark.

APPENDIX A
DERIVATION OF A NEW OPERATIONAL MATRIX OF INTEGRATION

Let $\mathbf{K}$ be an $(m+1)\times(m+1)$ operational matrix, then

$$\int_x^1 B^m(\tau)\mathrm{d}\tau \simeq \mathbf{K}B^m(x),\ x\in[0,1]$$

substituting (1) into the formulation, then

$$\begin{aligned}\int_x^1 B^m(\tau)\mathrm{d}\tau &= A\begin{bmatrix}1-x\\ \frac{1}{2}(1-x^2)\\ \vdots\\ \frac{1-x^{m+1}}{m+1}\end{bmatrix} = A\Lambda\Psi\begin{bmatrix}1\\ x\\ \vdots\\ x^{m+1}\end{bmatrix}\\ &= A\Lambda\Psi C B^m(x) = \mathbf{K}B^m(x)\end{aligned}$$

where $\mathbf{K}=A\Lambda\Psi C$,

$$A=\left[\,A_1,A_2,\cdots,A_{m+1}\,\right]^{\mathrm{T}},\ C=\left[\,A_1^{-1},A_2^{-1},\cdots,A_{m+1}^{-1},c_{m+1}\,\right]^{\mathrm{T}}$$

$$A_{i+1}=\left[\overbrace{0,\cdots,0}^{i\ elements},\tbinom{m}{i},(-1)^1\tbinom{m}{i}\tbinom{m-i}{1},\cdots,(-1)^{m-i}\tbinom{m}{i}\tbinom{m-i}{m-i}\right]$$

$$\Lambda=\begin{bmatrix}1&0&\cdots&0\\ 0&\frac{1}{2}&\cdots&0\\ \vdots&\vdots&\ddots&\vdots\\ 0&0&\cdots&\frac{1-x^{m+1}}{m+1}\end{bmatrix},\ \Psi=\begin{bmatrix}1&-1&0&\cdots&0\\ 1&0&-1&\cdots&0\\ \vdots&\vdots&\vdots&\ddots&\vdots\\ 1&0&0&\cdots&-1\end{bmatrix}.$$

In the light of Ref. [52], the elements c_{m+1} in matrix C is calculated as follow.

$$c_{m+1}=\frac{Q^{-1}}{2m+2}\left[\frac{\binom{m}{0}}{\binom{2m+1}{m+1}},\ \frac{\binom{m}{1}}{\binom{2m+1}{m+2}},\ \cdots\ \frac{\binom{m}{m}}{\binom{2m+1}{2m+1}}\right]^{\mathrm{T}}$$

where

$$Q=\langle B^m(x),B^m(x)\rangle=\int_0^1 B^m(x)[B^m(x)]^{\mathrm{T}}\mathrm{d}x=AHA^{\mathrm{T}}$$

$$H=\begin{bmatrix}1&\frac{1}{2}&\cdots&\frac{1}{m+1}\\ \frac{1}{2}&\frac{1}{3}&\cdots&\frac{1}{m+2}\\ \vdots&\vdots&\ddots&\vdots\\ \frac{1}{m+1}&\frac{1}{m+2}&\cdots&\frac{1}{2m+1}\end{bmatrix}$$

REFERENCES

[1] P. Mancarella, "Multi-energy systems: The smart grid beyond electricity," *LBL, Berkeley*, 2012.
[2] P. Mancarella, "Smart multi-energy grids: concepts, benefits and challenges," in *IEEE Power and Energy Society General Meeting*. IEEE, July 2012.
[3] P. Mancarella, "MES (multi-energy systems): An overview of concepts and evaluation models," *Energy*, vol. 65, pp. 1–17, 2014.
[4] P. Mancarella, G. Andersson, J. A. Peas-Lopes, and K. R. W. Bell, "Modelling of integrated multi-energy systems: Drivers, requirements, and opportunities," in *Power Systems Computation Conference (PSCC)*. IEEE, June 2016.
[5] T. Krause, G. Andersson, K. Frohlich, and A. Vaccaro, "Multiple-energy carriers: modeling of production, delivery, and consumption," *Proceedings of the IEEE*, vol. 99, no. 1, pp. 15–27, 2011.
[6] B. V. Mathiesen, H. Lund, D. Connolly *et al.*, "Smart energy systems for coherent 100% renewable energy and transport solutions," *Applied Energy*, vol. 145, pp. 139–154, 2015.
[7] E. Widl, T. Jacobs, D. Schwabeneder *et al.*, "Studying the potential of multi-carrier energy distribution grids: A holistic approach," *Energy*, vol. 153, pp. 519–529, 2018.
[8] "Short-Term Energy Outlook 2018," U.S. Energy Information Administration, Washington DC, US, Tech. Rep., January 2019. [Online]. Available: https://www.eia.gov/outlooks/steo
[9] "World Energy Investment 2018," International Energy Agency, Paris, France, Tech. Rep., July 2018.
[10] "World Energy Outlook 2018," International Energy Agency, Paris, France, Tech. Rep., Nov. 2018.
[11] M. Götz, J. Lefebvre, F. Mörs, A. M. Koch, F. Graf, S. Bajohr, R. Reimert, and T. Kolb, "Renewable power-to-gas: A technological and economic review," *Renewable energy*, vol. 85, pp. 1371–1390, 2016.
[12] A. Mazza, E. Bompard, and G. Chicco, "Applications of power to gas technologies in emerging electrical systems," *Renewable and Sustainable Energy Reviews*, vol. 92, pp. 794–806, 2018.
[13] M. Shahidehpour, Y. Fu, and T. Wiedman, "Impact of natural gas infrastructure on electric power systems," *Proceedings of the IEEE*, vol. 93, no. 5, pp. 1042–1056, 2005.
[14] M. Gil, P. Dueñas, and J. Reneses, "Electricity and natural gas interdependency: comparison of two methodologies for coupling large market models within the european regulatory framework," *IEEE Transactions on Power Systems*, vol. 31, no. 1, pp. 361–369, 2016.
[15] M. Shahidehpour and Z. Li, "White Paper: Long-term Electric and Natural Gas Infrastructure Requirements," Illinois Institute of Technology, Chicago, IL, USA, Tech. Rep., November 2014.
[16] C. A. Saldarriaga, R. A. Hincapi, and H. Salazar, "A holistic approach for planning natural gas and electricity distribution networks," *IEEE Transactions on Power Systems*, vol. 28, no. 4, pp. 4052–4063, 2013.
[17] J. Qiu, Z. Y. Dong, J. H. Zhao, K. Meng, Y. Zheng, and D. J. Hill, "Low carbon oriented expansion planning of integrated gas and power systems," *IEEE Transactions on Power Systems*, vol. 30, no. 2, pp. 1035–1046, 2015.
[18] T. Ding, Y. Hu, and Z. Bie, "Multi-stage stochastic programming with nonanticipativity constraints for expansion of combined power and natural gas systems," *IEEE Transactions on Power Systems*, vol. 33, no. 1, pp. 317–328, 2018.

[19] T. Li, M. Eremia, and M. Shahidehpour, "Interdependency of natural gas network and power system security," *IEEE Transactions on Power Systems*, vol. 23, no. 4, pp. 1817–1824, 2008.
[20] C. Liu, M. Shahidehpour, Y. Fu, Z. Li *et al.*, "Security-constrained unit commitment with natural gas transmission constraints," *IEEE Transactions on Power Systems*, vol. 24, no. 3, pp. 1523–1536, 2009.
[21] S. Badakhshan, M. Ehsan, M. Shahidehpour, N. Hajibandeh, M. Shafie-Khah, and J. P. S. Catalo, "Security-constrained unit commitment with natural gas pipeline transient constraints," *IEEE Transactions on Smart Grid*, vol. 11, no. 1, pp. 118–128, 2020.
[22] M. Qadrdan, J. Wu, N. Jenkins, and J. Ekanayake, "Operating strategies for a gb integrated gas and electricity network considering the uncertainty in wind power forecasts," *IEEE Transactions on Sustainable Energy*, vol. 5, no. 1, pp. 128–138, 2014.
[23] Q. Zeng, J. Fang, J. Li, and Z. Chen, "Steady-state analysis of the integrated natural gas and electric power system with bi-directional energy conversion," *Applied Energy*, vol. 184, pp. 1483 – 1492, 2016.
[24] Z. Zeng, T. Ding, Y. Xu, Y. Yang, and Z. Dong, "Reliability evaluation for integrated power-gas systems with power-to-gas and gas storages," *IEEE Transactions on Power Systems*, vol. 35, no. 1, pp. 571–583, 2020.
[25] F. Toledo, E. Sauma, and S. Jerardino, "Energy cost distortion due to ignoring natural gas network limitations in the scheduling of hydrothermal power systems," *IEEE Transactions on Power Systems*, vol. 31, no. 5, pp. 3785–3793, 2016.
[26] X. Zhang, M. Shahidehpour, A. Alabdulwahab, and A. Abusorrah, "Hourly electricity demand response in the stochastic day-ahead scheduling of coordinated electricity and natural gas networks," *IEEE Transactions on Power Systems*, vol. 31, no. 1, pp. 592–601, 2016.
[27] R. Z. Ríos-Mercado and C. Borraz-Sánchez, "Optimization problems in natural gas transportation systems: A state-of-the-art review," *Applied Energy*, vol. 147, pp. 536–555, 2015.
[28] C. M. Correa-Posada and P. Sánchez-Martín, "Integrated power and natural gas model for energy adequacy in short-term operation," *IEEE Transactions on Power Systems*, vol. 30, no. 6, pp. 3347–3355, 2015.
[29] M. Chaudry, N. Jenkins, and G. Strbac, "Multi-time period combined gas and electricity network optimisation," *Electric power systems Research*, vol. 78, no. 7, pp. 1265–1279, 2008.
[30] C. Liu, M. Shahidehpour, and J. Wang, "Coordinated scheduling of electricity and natural gas infrastructures with a transient model for natural gas flow," *Chaos: An Interdisciplinary Journal of Nonlinear Science*, vol. 21, no. 2, p. 025102, 2011.
[31] A. Zlotnik, L. Roald, S. Backhaus, M. Chertkov, and G. Andersson, "Coordinated scheduling for interdependent electric power and natural gas infrastructures," *IEEE Transactions on Power Systems*, vol. 32, no. 1, pp. 600–610, Jan 2017.
[32] J. Fang, Q. Zeng, X. Ai, Z. Chen, and J. Wen, "Dynamic optimal energy flow in the integrated natural gas and electrical power systems," *IEEE Transactions on Sustainable Energy*, vol. 9, no. 1, pp. 188–198, 2018.
[33] J. Yang, N. Zhang, C. Kang, and Q. Xia, "Effect of natural gas flow dynamics in robust generation scheduling under wind uncertainty," *IEEE Transactions on Power Systems*, vol. 33, no. 2, pp. 2087–2097, 2018.
[34] W. Liu, P. Li, W. Yang, and C. Chung, "Optimal energy flow for integrated energy systems considering gas transients," *IEEE Transactions on Power Systems*, vol. 34, no. 6, pp. 5076–5079, 2019.
[35] A. Zlotnik, M. Chertkov, and S. Backhaus, "Optimal control of transient flow in natural gas networks," in *2015 54th IEEE conference on decision and control (CDC)*. IEEE, 2015, pp. 4563–4570.
[36] M. Milligan, B. Frew, E. Zhou, and D. J. Arent, "Advancing system flexibility for high penetration renewable integration (chinese translation)," National Renewable Energy Lab.(NREL), Golden, CO (United States), Tech. Rep., 2015.
[37] H. Kondziella and T. Bruckner, "Flexibility requirements of renewable energy based electricity systems–a review of research results and methodologies," *Renewable and Sustainable Energy Reviews*, vol. 53, pp. 10–22, 2016.
[38] T. A. Deetjen, J. D. Rhodes, and M. E. Webber, "The impacts of wind and solar on grid flexibility requirements in the electric reliability council of texas," *Energy*, vol. 123, pp. 637–654, 2017.
[39] B. Mohandes, M. S. El Moursi, N. D. Hatziargyriou, and S. El Khatib, "A review of power system flexibility with high penetration of renewables," *IEEE Transactions on Power Systems*, 2019.
[40] Y. Xu, T. Ding, M. Qu, and P. Du, "Adaptive dynamic programming for gas-power network constrained unit commitment to accommodate renewable energy with combined-cycle units," *IEEE Transactions on Sustainable Energy*, vol. 11, no. 3, pp. 2028–2039, 2020.
[41] J. Liu, W. Yao, J. Wen, J. Fang, L. Jiang, H. He, and S. Cheng, "Impact of power grid strength and pll parameters on stability of grid-connected dfig wind farm," *IEEE Transactions on Sustainable Energy*, vol. 11, no. 1, pp. 545–557, 2020.
[42] N. Navid and G. Rosenwald, "Ramp capability product design for miso markets," *Market Development and Analysis*, 2013.
[43] M. Parvania and A. Scaglione, "Unit commitment with continuous-time generation and ramping trajectory models," *IEEE Transactions on Power Systems*, vol. 31, no. 4, pp. 3169–3178, 2016.
[44] A. Nikoobakht, J. Aghaei, M. Shafie-Khah, and J. P. S. Catalo, "Continuous-time co-operation of integrated electricity and natural gas systems with responsive demands under wind power generation uncertainty," *IEEE Transactions on Smart Grid*, vol. 11, no. 4, pp. 3156–3170, 2020.
[45] M. Parvania and R. Khatami, "Continuous-time marginal pricing of electricity," *IEEE Transactions on Power Systems*, vol. 32, no. 3, pp. 1960–1969, 2017.
[46] B. Xia, H. Wu, Y. Qiu, B. Lou, and Y. Song, "A galerkin method-based polynomial approximation for parametric problems in power system transient analysis," *IEEE Transactions on Power Systems*, vol. 34, no. 2, pp. 1620–1629, 2019.
[47] D. Xiu and G. E. Karniadakis, "Modeling uncertainty in flow simulations via generalized polynomial chaos," *Journal of computational physics*, vol. 187, no. 1, pp. 137–167, 2003.
[48] L. Tang and W. Sun, "An automated transient stability constrained optimal power flow based on trajectory sensitivity analysis," *IEEE Transactions on Power Systems*, vol. 32, no. 1, pp. 590–599, 2017.
[49] H. Wu, Y. Zhou, S. Dong, and Y. Song, "Probabilistic load flow based on generalized polynomial chaos," *IEEE Transactions on Power Systems*, vol. 32, no. 1, pp. 820–821, 2017.
[50] P. Dierckx, *Curve and surface fitting with splines*. New York, USA: Oxford University Press, 1995.
[51] E. V. Shikin and A. I. Plis, *Handbook on Splines for the User*. Boca Raton, FL, USA: CRC Press, 1995.
[52] S. Yousefi and M. Behroozifar, "Operational matrices of bernstein polynomials and their applications," *International Journal of Systems Science*, vol. 41, no. 6, pp. 709–716, 2010.
[53] A. Thorley and C. Tiley, "Unsteady and transient flow of compressible fluids in pipelinesa review of theoretical and some experimental studies," *International journal of heat and fluid flow*, vol. 8, no. 1, pp. 3–15, 1987.
[54] A. Osiadacz, *Simulation and analysis of gas networks*. Houston, TX, USA: Gulf Publishing Company, 1987.
[55] M. Carrión and J. M. Arroyo, "A computationally efficient mixed-integer linear formulation for the thermal unit commitment problem," *IEEE Transactions on Power Systems*, vol. 21, no. 3, pp. 1371–1378, 2006.
[56] D. De Wolf and Y. Smeers, "The gas transmission problem solved by an extension of the simplex algorithm," *Management Science*, vol. 46, no. 11, pp. 1454–1465, 2000.
[57] Energinet, Denmark. Energi Data Service. [Online]. Available: http://www.energidataservice.dk

Chao Zheng received the B.Eng. and Ph.D. degrees from the School of Electrical and Electronic Engineering, Huazhong University of Science and Technology, Wuhan, China, in 2014 and 2020, respectively. He was a joint/guest Ph.D. student with the Department of Energy Technology, Aalborg University, Aalborg, Denmark, from 2018 to 2019. He is currently an independent system operator in the Electric Power Dispatch and Control Center, Yunnan Power Grid Co. Ltd, Kunming, China.

His main research interests include deep learning applications for power systems, power system operation and control, and optimal energy flow of the integrated power and gas systems.

Jiakun Fang (SM'19) received the B.Sc. and Ph.D. degrees from the Huazhong University of Science and Technology, Wuhan, China, in 2007 and 2012, respectively. From 2012 to 2019, he was with the Department of Energy Technology, Aalborg University, Aalborg, Denmark. He is currently a Professor with the School of Electrical and Electronics Engineering, Huazhong University of Science and Technology, Wuhan, China.

His main research interests include the integrated oil, gas and power systems for bulk energy transmission and storage across multiple energy carriers.

Shaorong Wang received the B.Eng. degree from Zhejiang University, Hangzhou, China, in 1984, the M.S. degree from North China Electric Power University, Baoding, China, in 1990, and the Ph.D. degree from the Huazhong University of Science and Technology, Wuhan, China, in 2004. He is currently a Professor with the School of Electrical and Electronic Engineering, Huazhong University of Science and Technology, Wuhan, China.

His main research interests include power system operation and control, smart grid, robotic application, big data, and machine vision.

Xiaomeng Ai (M'17) received the B.Eng. degree in mathematics and applied mathematics and the Ph.D. degree in electrical engineering from the Huazhong University of Science and Technology (HUST), Wuhan, China, in 2008 and 2014, respectively. He is currently a Lecturer with HUST.

His main research interests include the theory about continuous-time optimization with uncertainties in power systems, renewable energy integration, and integrated energy market.

Zhou Liu ((SM'20)) received the Ph.D. degree in energy technology from Aalborg University, Aalborg, Denmark, in 2013. Since December 2014, he has been a Postdoc Researcher with the Department of Electrical Power Engineer, Norwegian University of Science and Technology, Trondheim, Norway. From 2017 to 2018, he was a Postdoc Fellow with the Department of Electrical Sustainable Energy, TU Delft, Delft, the Netherlands. He is currently an Assistant Professor with the Department of Energy Technology, Aalborg University.

His main research interests include power system protection, power system stability and control, energy system integration, digital substation, and smart grid technology.

Zhe Chen (F'19) received the B.Eng. and M.Sc. degrees from the Northeast China Institute of Electric Power Engineering, Jilin City, China, in 1982 and 1986, respectively, and the Ph.D. degree from the University of Durham, Durham, U.K., in 1997.

He is currently a Full Professor with the Department of Energy Technology, Aalborg University, Aalborg, Denmark. He is also the Leader of the Wind Power System Research Program with the Department of Energy Technology, Aalborg University and the Danish Principle Investigator for Wind Energy of the Sino-Danish Centre for Education and Research. He has more than 400 publications in his technical field. His research areas include power systems, power electronics, and electric machines, and his main current research interests include wind energy and energy system integration.

Dr. Chen is an Editor for the IEEE TRANSACTIONS ON POWER SYSTEMS, an Associate Editor for the IEEE TRANSACTIONS ON POWER ELECTRONICS, a Fellow of the Institution of Engineering and Technology, London, U.K., and a Chartered Engineer in the U.K.